

High-Fidelity GAN Inversion for Image Attribute Editing

Tengfei Wang¹, Yong Zhang^{2†}, Yanbo Fan², Jue Wang², Qifeng Chen^{1†}

¹The Hong Kong University of Science and Technology

²Tencent AI Lab

Abstract

We present a novel high-fidelity generative adversarial network (GAN) inversion framework that enables attribute editing with image-specific details well-preserved (e.g., background, appearance and illumination). We first formulate GAN inversion as a lossy data compression problem and carefully discuss the Rate-Distortion-Edit trade-off. Due to this trade-off, previous works fail to achieve high-fidelity reconstruction while keeping compelling editing ability with a low bit-rate latent code only. In this work, we propose a distortion consultation approach that employs the distortion map as a reference for reconstruction. In the distortion consultation inversion (DCI), the distortion map is first projected to a high-rate latent map, which then complements the basic low-rate latent code with (lost) details via consultation fusion. To achieve high-fidelity editing, we propose an adaptive distortion alignment (ADA) module with a self-supervised training scheme. Extensive experiments in the face and car domains show a clear improvement in terms of both inversion and editing quality. Our project page is at <https://tengfei-wang.github.io/HFGI/>.

1 Introduction

Image attribute editing is the task of modifying desired attributes of a given image while preserving other details. With the rapid advance of generative adversarial networks (GANs) (Goodfellow et al. 2014), a promising direction is to manipulate images with the phenomenal realism and strong control capacity of StyleGAN (Karras, Laine, and Aila 2019; Karras et al. 2020). To enable real-world image editing, GAN inversion techniques (Xia et al. 2021) have been recently explored, which aim at projecting images to the latent space of a well-trained GAN generator.

Existing GAN inversion approaches either perform per-image optimization (Zhu et al. 2016; Abdal, Qin, and Wonka 2019; Kang, Kim, and Cho 2021) or learn a data-driven encoder (Richardson et al. 2021; Tov et al. 2021). Optimization approaches achieve faithful inversion but would overfit on a single image, leading to inferior editing quality. In contrast, encoder methods are faster and show superior editing performance benefiting from general knowledge learned on numerous images. Nevertheless, their reconstruction results are usually inaccurate and of low fidelity since the training tends

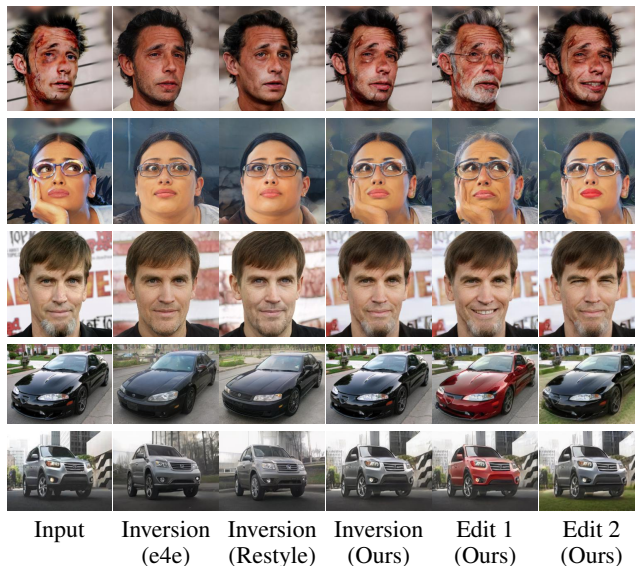


Figure 1: High-fidelity image inversion and editing (age, smile, lip, eyes, color, grass). Our method is robust to occlusion and performs well on detail preservation such as background, makeup, beard/hair style, reflection and shadow.

to compromise among all training images and converge to the averaged area. These methods can reconstruct a coarse layout (low-frequency patterns), but the image-specific details (high-frequency patterns) are often ignored. For example, the reconstructed face images typically possess averaged patterns that agree with the majority of training images (e.g., normal pose/expression, occlusion/shadow-free), and the details that present minority patterns (e.g., background, illumination, accessory) in training data are subject to distortion. On top of inversion, it is also desirable to preserve these image-specific details in editing images with high fidelity.

Though some works tried to improve the reconstruction accuracy of encoder-based methods, their editing performance usually decreases (Tov et al. 2021). To theoretically analyze the limitation of existing approaches, we reformulate the GAN inversion problem as a lossy data compression system with a frozen decoder. According to Rate-Distortion theory (Shannon et al. 1959), reversing a real-world image

[†]Corresponding Authors.

to a low-dimensional latent code would inevitably lead to information loss. As conjectured by information bottleneck theory (Tishby and Zaslavsky 2015), the lost information is primarily image-specific details as the deep compression model tends to retain common information of a domain. Based on these analyses and experimental observations, we present the **Rate-Distortion-Edit trade-off** for GAN inversion, which further inspires our framework.

According to this Rate-Distortion-Edit trade-off, the low-rate latent codes are insufficient for high-fidelity inversion and editing. We, therefore, propose a novel framework that improves encoder models with **distortion consultation**. The consultation branch serves as a ‘cheat sheet’ for reconstruction that explicitly conveys the ignored image-specific information. Specifically, we leverage the distortion map between source and low-fidelity reconstructed image as a reference and project it to higher-rate latent maps. The high-rate latent map and low-rate latent code are further embedded and fused in the generator via the **consultation fusion** module. Our scheme shows a clear improvement in reconstruction quality, and no test-time optimization is involved.

For attribute editing, we perform vector arithmetic (Radford, Metz, and Chintala 2016) on the low-rate latent code, and the latent map is desired to bring back lost details. While the distortion consultation substantially contributes to the inversion quality, it is non-trivial to propagate the distortion map observed on the inversion image for editing due to the misalignment between inverted and edited images. To this end, we additionally design an **adaptive distortion alignment (ADA)** network to adjust the distortion map with the edited images. To disentangle the alignment from the consultation encoder and stabilize the training, we impose intermediate supervision on ADA by proposing an alignment regularization with a self-supervised training scheme.

Extensive experiments show that our method significantly outperforms state-of-the-art encoder-based approaches in terms of both reconstruction and editing performance. On account of the high-fidelity inversion capacity, our approach is robust to viewpoint and illumination fluctuation and can thus perform temporally consistent editing on videos. Our primary contributions can be summarized as follows.

- We formulate GAN inversion as a data compression problem and present the trade-off among the bit-rate of latent codes, reconstruction quality and editing quality.
- We propose the distortion consultation module and adaptive distortion alignment module, which are designed for high-fidelity inversion and editing.
- Our method outperforms state-of-the-art approaches qualitatively and quantitatively on diverse image domains and videos. The framework is simple and can be easily applied to GAN models.

2 Related Work

2.1 GAN Inversion

Existing GAN inversion approaches can be categorized into optimization-based, encoder-based, and hybrid methods. Optimization approaches can achieve high reconstruction quality but are slow for inference. Zhu et al. (2016)

used L-BFGS, and I2S (Abdal, Qin, and Wonka 2019) adopted ADAM for solving the optimization. Huh et al. (2020) adopted Covariance Matrix Adaptation for gradient-free optimization. Instead of per-image optimization, Zhu et al. (2016) learned an encoder to project images. Zhu et al. (2020a) proposed an in-domain method on real images. pSp (Richardson et al. 2021) and (Xu et al. 2021) proposed to embed latent codes in a hierarchical manner. Further, e4e (Tov et al. 2021) analyzed the trade-offs between reconstruction and editing ability. Wei et al. (2021) improved the inversion efficiency by a shallow network with efficient heads. ReStyle (Alaluf, Patashnik, and Cohen-Or 2021) projected the latent codes with iterative refinements. These methods are more efficient but fail to achieve high-fidelity reconstruction. Hybrid approaches make a compromise. Zhu et al. (2016) initialize the optimization with the encoder output for acceleration. Guan et al. (2020) designed a collaborative learning scheme for encoder and optimization iterator. Compared with previous methods, our method considerably improves the reconstruction quality of encoder models without inference-time optimization.

GAN inversion approaches can also be classified by the used latent space. **Z** space (Karras, Laine, and Aila 2019) is straightforward but suffers from feature entanglement. **W** and **W**⁺ (Abdal, Qin, and Wonka 2019, 2020) space in StyleGAN are more disentangled, where **W**⁺ space extends **W** space by using different *W* across layers. **S** space (Wu, Lischinski, and Shechtman 2021) is proposed by transforming **W**⁺ through the affine layers. **P** space (Zhu et al. 2020b) inverts images to the last activation layer in the non-linear mapping network. Besides StyleGAN, multi-code GAN (Gu, Shen, and Zhou 2020) also adopts multi-scale latent codes for ProgressGAN (Karras et al. 2018). Nevertheless, these latent spaces would inevitably lose details in reconstructed images due to limited bit-rate (See Sec.3). To perform a high-fidelity inversion, we propose a distortion consultation branch to convey high-frequency image-specific information.

2.2 Latent Space Editing

A number of supervised and unsupervised approaches explored GAN latent space for semantic directions under the vector arithmetic. The supervised methods need off-the-shelf attribute classifiers or annotated images for specific attributes. InterfaceGAN (Shen et al. 2020) trained SVM to learn the boundary hyperplane for each binary attribute. StyleFlow (Abdal et al. 2021) learned reversible mapping by normalizing flow and off-the-shelf classifiers. Others (Jahanian, Chai, and Isola 2020; Plumerault, Borgne, and Hudelot 2020) explored simple geometric transformation via self-supervised learning. Unsupervised approaches do not need pre-trained classifiers. GANspace (Harkonen et al. 2020) performed principal components analysis (PCA) on early feature layers. Similarly, SeFa (Shen et al. 2020) performed eigenvector decomposition of the affine layers. Some works (Voynov and Babenko 2020; Lu et al. 2020; Zhuang, Koyejo, and Schwing 2021) found distinguishable directions based on mutual information. LatentCLR (Yuksel et al. 2021) explored directions by contrastive learning.

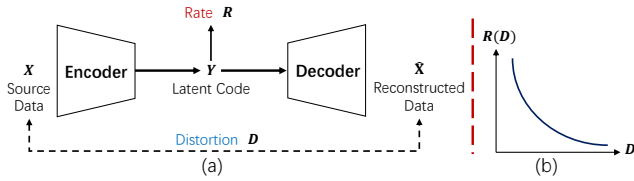


Figure 2: (a) Illustration of the data compression system and (b) Rate-Distortion trade-offs.

3 Motivation

3.1 Background

Rate-Distortion Theory. The Rate-Distortion theory (Shannon et al. 1959; Cover 1999; Blau and Michaeli 2019) presents an analytical expression for the trade-off between the bit-rate and reconstruction quality of data compression. Fig. 2 demonstrates a typical system of lossy data compression, where *rate* indicates the bit length (size) of the latent code Y while *distortion* reflects the fidelity of reconstructed data. The distortion D is measured by $D = \mathbb{E}[\Delta(X, \hat{X})]$, where Δ is ℓ_1 loss in our case. Given a maximum distortion D^* , the lower-bound for the bit-rate R is given by:

$$R(D^*) = \min_{D \leq D^*} \{I(X; \hat{X})\}, \quad (1)$$

where $I(\cdot)$ denotes the mutual information.

Information Bottleneck Theory. Rate-Distortion theory determines the level of inevitable distortion D with a specific rate R . Information Bottleneck theory (Tishby, Pereira, and Bialek 1999; Tishby and Zaslavsky 2015; Shwartz-Ziv and Tishby 2017) further extends it without explicitly defining the distortion function:

$$R = \min\{I(X; Y) - \beta I(Y; \hat{X})\}. \quad (2)$$

This theory further conjectures that the training process of deep models consists of two stages. The network first fits on the training data, where $I(Y; \hat{X})$ increases and then forgets minor information, where $I(X; Y)$ decreases. This observation implies the essential role of forgetting in learning, and the deep model thus primarily learns common patterns of the training data for reconstruction. In contrast, infrequent patterns and image-specific details are typically forgettable trivialities for the trained models.

3.2 Rate-Distortion Trade-offs in GAN Inversion

We formulate the encoder-based GAN inversion as a problem of lossy data compression. As shown in Fig. 3 (a), the decoder is a frozen well-trained generator (e.g., StyleGAN), and the encoder learns a mapping from the source image to the latent codes. In this formulation, *rate* can be interpreted as the dimension of latent codes (e.g., 18×512), and *distortion* indicates the reconstruction quality (fidelity). A compelling inversion method is desired to produce high-fidelity images for both inversion and editing (*low distortion*). Nevertheless, the dimension of latent codes is much smaller than that of images (*low rate*). This implies a contradiction with (Shannon et al. 1959; Tishby, Pereira, and Bialek 1999). As

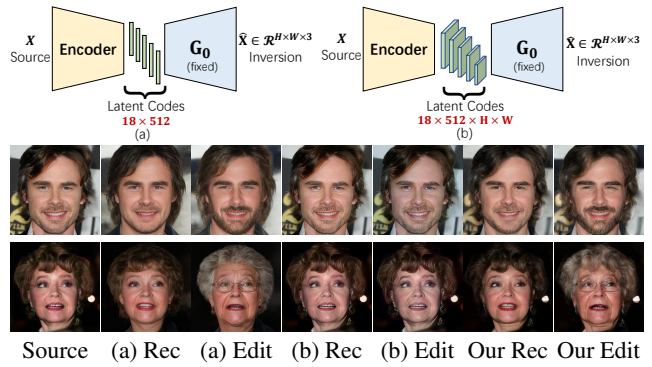


Figure 3: Rate-Distortion-Edit trade-offs. (a) is a typical framework for GAN inversion but suffers detail loss and reconstruction distortion with low-rate latent codes. (b) is a typical framework for image restoration but suffers inferior interpretability and editability with high-rate latent codes.

observed in previous GAN inversion results, some image-specific details such as background, appearance and illumination are inevitably lost. This shows the low-rate latent codes are insufficient for high-fidelity GAN inversion.

3.3 Rate-Distortion-Edit Trade-offs

We further discuss the *Rate-Distortion-Edit* trade-offs in this section. A naive idea for faithful reconstruction is to adopt a higher-rate latent code like Fig. 3 (b). However, it is non-trivial to reduce the distortion by increasing the latent rate. Some image restoration works (Chen et al. 2021; Wang et al. 2021) adopt an Unet-like structure in Fig. 3 (b) that conveys latent maps (e.g., $18 \times 512 \times H \times W$) to decoder. Benefited from the higher bit rate, the restoration quality is gratifying. However, we cannot apply this in our case since the high-dimensional latent codes are difficult to interpret and manipulate for attribute editing. Similarly, prior work (Tov et al. 2021) also observed tradeoffs between the reconstruction and editability for case (a). As the inversion is just an intermediate step to achieve the goal of editing, it is essential to balance the rate, reconstruction, and editing quality. To this end, we propose a distortion consultation branch to supplement image-specific details while still perform editing (add a semantic vector) on the low-rate latent code.

4 Approach

4.1 Overview

Given a source image X and a well-trained generator G_0 , GAN inversion infers the latent code W via an encoder E_0 , which is expected to faithfully reconstruct X . As the basic encoder E_0 is trained to minimize reconstruction errors for all training images, it tends to retain low-frequency (common) information while filtering out high-frequency (image-specific) details. Different from previous works that rely on E_0 only, we propose a distortion consultation branch to convey image-specific details for high-fidelity inversion (Sec. 4.2), as shown in Fig. 4. To perform editing, we also propose an adaptive distortion alignment module (Sec. 4.3).

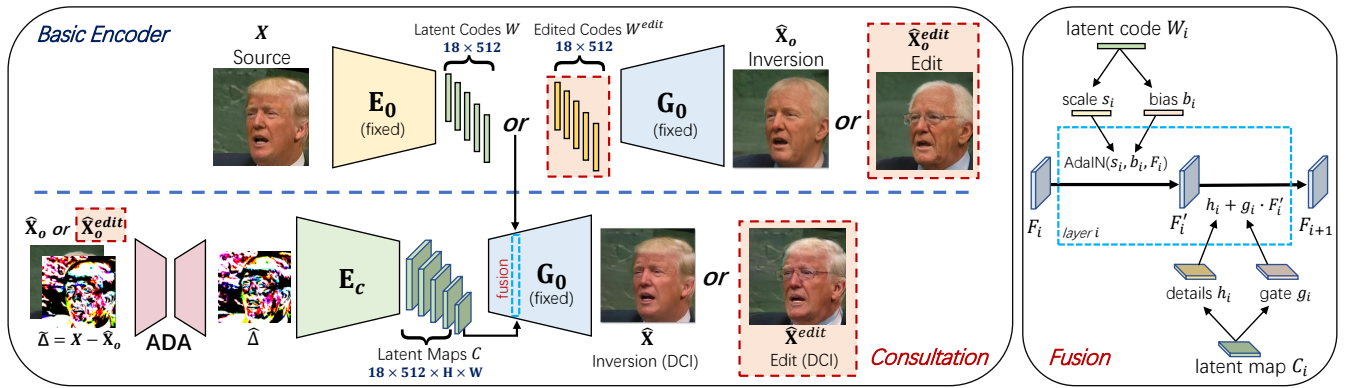


Figure 4: Overview of our high-fidelity image inversion and editing framework. The basic encoder E_0 infers a low-rate latent code W corresponding to a low-fidelity reconstruction image \hat{X}_o . The distortion map $\tilde{\Delta}$ between \hat{X}_o and the source image X contains the lost high-frequency image-specific details to improve the reconstruction fidelity. The red dotted boxes indicate the editing behaviour with certain semantic direction N^{edit} , where $W^{edit} = W + \alpha N^{edit}$ corresponds to a low-fidelity editing image \hat{X}_o^{edit} . To achieve high-fidelity image editing, we propose the distortion consultation branch to facilitate the generation. In the distortion consultation, $\tilde{\Delta}$ is first aligned with the low-fidelity edited image \hat{X}_o^{edit} by ADA and then embedded to a high-rate latent map C via the consultation encoder E_c . Latent code W and latent map C are combined via the consultation fusion (see details in the right part) across layers of G_0 to generate the final edited image \hat{X}^{edit} .

4.2 Distortion Consultation Inversion (DCI)

Basic Encoder. With a basic encoder E_0 , we can obtain a low-rate latent code $W = E_0(X)$ and initial inversion image $\hat{X}_o = G_0(W)$. In this case, the StyleGAN generator G_0 takes W as the input in each layer to obtain the feature map:

$$F_{i+1} = AdaIN(F_i, f_i^s(W_i), f_i^b(W_i)), \quad (3)$$

where $f_i^s(W_i), f_i^b(W_i)$ are affine layers for scale and bias in $AdaIN(\cdot)$. \hat{X}_o is usually low-fidelity due to the information loss of low-rate latent codes, and the subscript o denotes an (unsatisfactory) observation of source image X .

Consultation Encoder. To enhance E_0 with higher fidelity, we propose a distortion consultation branch to convey the lost image-specific details. We refer it to *Consultation*, since the network explicitly consults the image-specific information as a reference for generation. Specifically, we see the distortion map $\tilde{\Delta} = X - \hat{X}_o$ between source X and initial reconstruction \hat{X}_o as the lost details. The distortion map is projected to a high-rate latent map $C = E_c(\tilde{\Delta})$ via the consultation encoder E_c . Compared with prior methods relying on W only, G_0 additionally consults C for lost details to achieve high-fidelity reconstruction as $\hat{X} = G_0(W, C)$.

Consultation Fusion. To combine the consultation branch with the basic encoder for image generation, we adopt a layer-wise consultation fusion for latent codes W and latent maps C , as shown in Fig. 4. As artifacts and inaccurate details introduced by W can degrade the generation quality, we design a gated fusion scheme to adaptively filter out undesired features. In layer i of G_0 , C_i is embedded to a gate map g_i and a high-frequency details map h_i as:

$$g_i = f_i^{gate}(C_i), h_i = f_i^{hf}(C_i), \quad (4)$$

where mapping functions f_i^{gate} and f_i^{hf} are convolution layers. h_i contains the image-specific details, and facilitates the

low-fidelity features obtained from W_i (eq. (2)) to produce high-fidelity feature maps F_{i+1} in StyleGAN as:

$$F_{i+1} = g_i \cdot AdaIN(F_i, f_i^s(W_i), f_i^b(W_i)) + h_i. \quad (5)$$

To avoid overfitting on the inversion result, we only perform the consultation fusion in early layers of G_0 .

4.3 Adaptive Distortion Alignment (ADA)

For attribute editing, the low-rate latent code W would be moved along certain semantic direction N^{edit} as $W^{edit} = W + \alpha N^{edit}$ (Shen et al. 2020). The initial edited image by the basis encoder is denoted as $\hat{X}_o^{edit} = G_0(W^{edit})$, which suffers details distortion. So far, we have improved the fidelity of the inversion image \hat{X}_o with the proposed DCI, where the distortion map $\tilde{\Delta} = X - \hat{X}_o$ is calculated for \hat{X}_o . However, \hat{X}_o^{edit} would be deformed from \hat{X}_o when editing attributes such as age, pose and expression. This means the observed $\tilde{\Delta}$ may not align with the edited image \hat{X}_o^{edit} . Applying DCI directly to \hat{X}_o^{edit} leads to obvious artifacts by consulting misaligned details $\tilde{\Delta}$ (see Sec.5.3). To advance DCI from inversion to editing, the observed distortion map $\tilde{\Delta}$ is supposed to be adaptively aligned with the edited image \hat{X}_o^{edit} . We thus propose the ADA module, which is an encoder-decoder-like structure for distortion alignment.

Considering a misaligned pair of $\{I, \tilde{\Delta}\}$ where I is \hat{X}_o for inversion and \hat{X}_o^{edit} for editing, ADA is to align the distortion map $\tilde{\Delta}$ with a target image I . For inversion, ADA is ideally an identity mapping. For editing, the distortion map is desired to be adaptively transformed as $\tilde{\Delta}^{edit} = ADA(\hat{X}_o^{edit}, \tilde{\Delta})$ that aligns with the initial editing result \hat{X}_o^{edit} . With $C^{edit} = E_c(\tilde{\Delta}^{edit})$ as a reference, $\hat{X}^{edit} = G_0(W^{edit}, C^{edit})$ can preserve more details.

Self-supervised Training. To alleviate the entanglement between distortion alignment and distortion consultation, involving intermediate supervisions on ADA outputs is preferred. To this end, we need numerous misaligned pairs of $\{I, \tilde{\Delta}\}$ and their ground-truth aligned maps Δ for training, but the data collection is labor-intensive. To conduct a self-supervised training, we take X as the source image, and the low-fidelity inversion \hat{X}_o as the target image I for alignment, and the ground-truth distortion is thus $\Delta = X - \hat{X}_o$. During the training, we augment Δ with random perspective transformation to simulate misaligned distortion maps $\tilde{\Delta}$. We empirically observe these simulated pairs work well on training and expect a better simulation scheme in future works. The ADA module is encouraged to produce the aligned distortion $\hat{\Delta} = ADA(\hat{X}_o, \tilde{\Delta})$ that approximates Δ . The alignment loss is defined as: $\mathcal{L}_{align} = \|\hat{\Delta} - \Delta\|_1$.

4.4 Losses

During the training, the generator G_0 and basic encoder E_0 are frozen. For faithful reconstruction, we calculate L_2 loss and LPIPS (Zhang et al. 2018) between \hat{X} and X . We also calculate the identity loss $\mathcal{L}_{id} = 1 - \langle F(X), F(\hat{X}) \rangle$, where F is pre-trained ArcFace (Deng et al. 2019) or a ResNet-50 model for different domains (Tov et al. 2021). The reconstruction loss is as: $\mathcal{L}_{rec} = \mathcal{L}_2 + \lambda_{per} \mathcal{L}_{LPIPS} + \lambda_{id} \mathcal{L}_{id}$. We also impose adversarial loss to improve image qualities:

$$\mathcal{L}_D = \mathbb{E}[\log D(\hat{X})] + \mathbb{E}[\log(1 - D(X))], \quad (6)$$

$$\mathcal{L}_{adv} = -\mathbb{E}[\log(D(\hat{X}))], \quad (7)$$

where D is initialized with the well-trained discriminator. In summary, the overall loss is a weighted summation of \mathcal{L}_{rec} , \mathcal{L}_{adv} and \mathcal{L}_{align} .

Note that the training only involves the inversion images, and no editing direction N^{edit} is needed in the training. After training, the model can generalize to diverse attribute editing explored by different methods.

5 Experiments

5.1 Settings

Datasets. For the human face domain, we use FFHQ (Karras, Laine, and Aila 2019) for training and CelebA-HQ (Karras et al. 2018) for cross-dataset evaluation. For the car domain, we use Stanford Cars (Krause et al. 2013) for training and evaluation. For attribute editing, we adopt InterfaceGAN for face images and GANSpace for car images.

Implementations. We use pretrained StyleGAN2 (Karras et al. 2020) as the generator, and e4e (Tov et al. 2021) as the basic encoder E_0 in all our experiments. We adopt Adam optimizer (Kingma and Ba 2015) with LookAhead (Zhang et al. 2019). The learning rate is set to $1e - 4$. The iteration number is set to 90,000 with a batch size of 8.

5.2 Evaluation

Quantitative Evaluation. We compare our method (with e4e as the basic encoder) with state-of-the-art encoder-based GAN inversion approaches, pSp (Richardson et al. 2021),

Method	MAE ↓	SSIM ↑	LPIPS ↓	Time ↓
Optimization*	.0610±.0004	.875±.005	.126±.003	127s
pSp	.0789±.0006	.793±.006	.169±.002	0.11s
Restyle _{pSp}	.0729±.0005	.823±.004	.145±.002	0.46s
e4e	.0919±.0008	.742±.007	.221±.003	0.11s
Restyle _{e4e}	.0887±.0008	.758±.007	.202±.003	0.46s
Ours _{e4e}	.0617±.0004	.877±.002	.127±.001	0.24s

Table 1: Quantitative comparison for inversion quality on faces.

Methods	Ours > pSp	Ours > e4e	Ours > Restyle
Preference Rate	80.6%	84.7%	79.5%

Table 2: The results of the user study. The reported value indicates the preference rate of Ours against a baseline.

e4e (Tov et al. 2021) and Restyle (Alaluf, Patashnik, and Cohen-Or 2021) (with pSp and e4e as backbones, respectively). We report quantitative comparisons of the inversion performance in Table 1. The metrics are calculated on the first 1,500 images from CelebA-HQ. We also compare the proposed method with the optimization-based approach (Abdal, Qin, and Wonka 2019). Note that the optimization method is only evaluated on a subset of 100 images due to the slow inference. Our approach substantially outperforms encoder-based baselines in terms of reconstruction quality and is considerably faster than optimization-based methods when inference.

Qualitative Evaluation. We show visual results of both inversion and editing in Fig. 5. Compared with previous approaches, our method is robust to images with occlusion and extreme viewpoints. For example, the first row in Fig. 5 gives a face image occluded by the hand, and the last row demonstrates a car image with an out-of-range viewpoint. Existing methods fail to faithfully reconstruct these challenging images. They generate distorted results and suffer artifacts for both inversion and editing. In contrast, with the proposed distortion consultation scheme, our method is more robust and thus produces compelling and high-fidelity results. Besides the robustness improvement, our approach also successfully preserves more details in terms of backgrounds (e.g., 4th row), shadow (e.g., 2nd row), reflect (e.g., 10th row), accessory (e.g., 5th row), expressions (e.g., 7th and 8th rows), and appearance (e.g., 9th row, 11th row). In contrast, previous encoder-based approaches inevitably lose some image-specific details with a low-rate inversion mechanism. More comparison results on the inversion and diverse attribute editing are given in the **Appendix**.

User Study. To perceptually evaluate the editing performance, we conduct a user study in Table 2. We select the first 50 images from the CelebA-HQ and perform editing on extensive attributes. We collect 800 votes from 16 participants. Each participant is given a triple of images (source, our editing, baseline editing) at once and asked to choose the higher-fidelity one with proper editing. The user study shows our method outperforms baselines by a large margin.

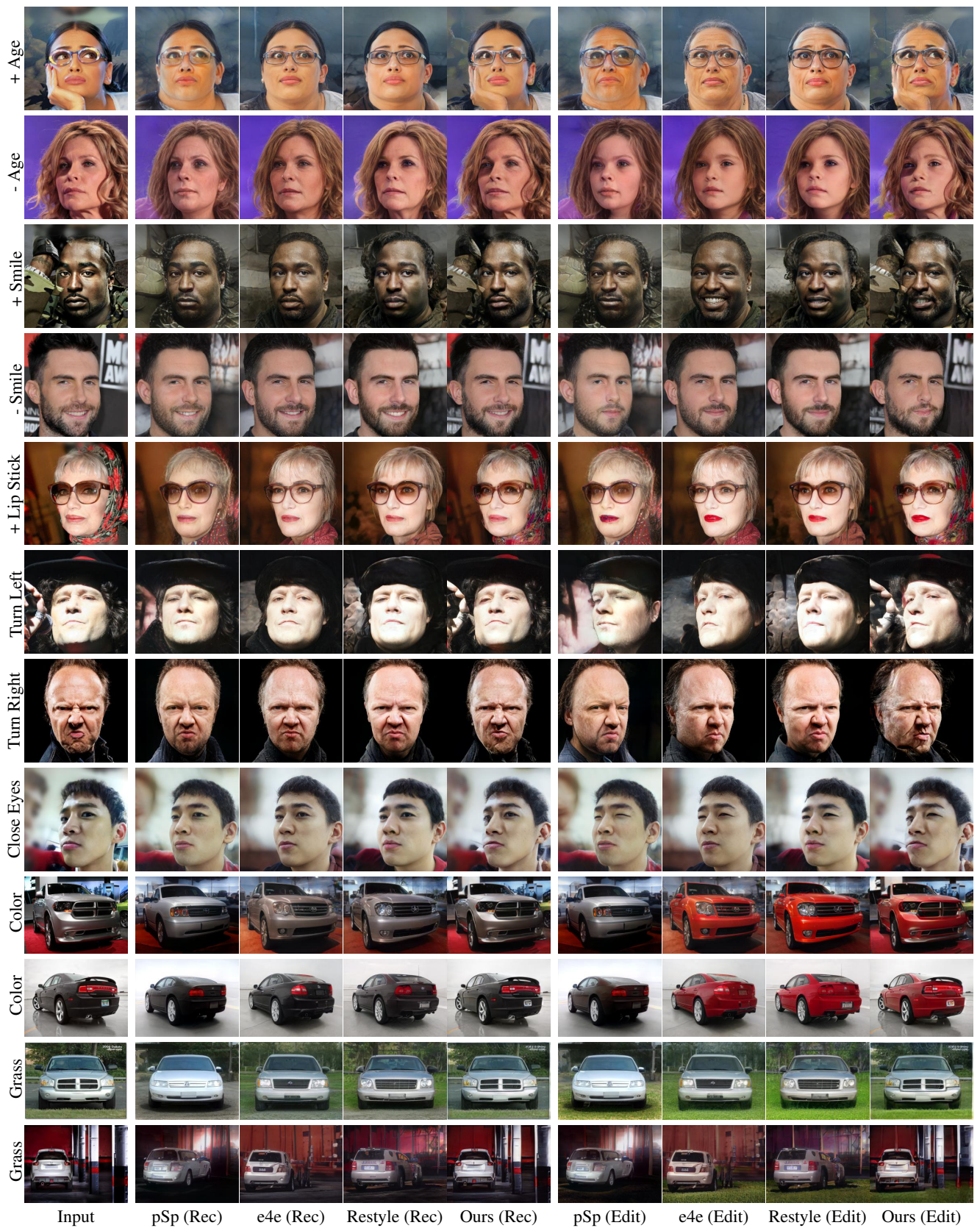


Figure 5: Visual comparisons on Face inversion and editing. More results are shown in **Appendix**.



Figure 6: Ablation study on the DCI. We show inversion results w/ and w/o DCI.

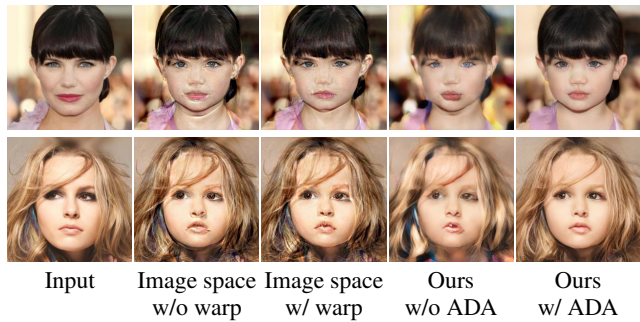


Figure 7: Ablation study on ADA. We integrate the distortion map in the image and feature space respectively and show the editing results.

5.3 Ablation Study

Effect of Distortion Consultation. As discussed before, the distortion consultation brings back ignored image details for reconstruction, complementing the low-rate basic encoder. To validate the effectiveness of the distortion consultation branch, we show our inversion results with and without DCI in Fig. 6. With the proposed distortion consultation branch, the model is more robust to occlusion and extreme poses and keeps more details in the reconstruction results.

Effect of Adaptive Distortion Alignment. To analyze the effect of ADA, we show the editing results with and without ADA in Fig. 7. Without the adaptive alignment, the distortion map fails to generalize to the edited image and degrades the generated image quality. In the proposed method, the aligned distortion map is embedded and integrated in the feature space via consultation encoding and consultation fusion. A naive alternative is to directly add the distortion map $\tilde{\Delta}$ to X_o^{edit} in the image space with warping estimated by face landmarks (Bulat and Tzimiropoulos 2017; Guo et al. 2020). As shown in Fig. 7, performing warping and fusion in the image space also leads to obvious artifacts, where the warping is implemented by coordinates interpolation of sparse facial landmarks.



Figure 8: Inversion and editing results on a real video.

5.4 Application

Real-world Video Editing. Compared with image inversion and editing, the key challenge for the video counterpart is the temporal consistency of details across frames. This puts a higher demand for the reconstruction fidelity since the distortion of every single image would be magnified in a video in terms of consistency and quality. We show inversion and editing results on a real video (Rossler et al. 2019) in Fig. 8. Previous low-rate inversion approaches lack robustness to pose variation, and fail to preserve the identity of the original person and suffer notable distortion in editing results. As the pose and viewpoint change across video frames, their results show inconsistent details and abrupt identity discrepancy. In contrast, the proposed method is more robust to cross-frame discrepancy (e.g., pose, viewpoint) and achieves higher fidelity for details preservation.

6 Conclusion

In this work, we propose a novel GAN inversion framework that enables high-fidelity image attribute editing. Considering the Rate-Distortion-Edit trade-off, we consult the observed distortion map as a high-rate reference to enhance the basic encoder model with high-quality reconstruction. With the adaptive distortion alignment and distortion consultation technique, our method is more robust to challenging cases such as images with occlusion and extreme viewpoints. Benefiting from the additional information conveyed by the consultation branch, the proposed scheme shows clear improvements in terms of image-specific details preservation (e.g., background, appearance and illumination) for both reconstruction and editing. Our method also performs well on video editing with consistent identity and details due to the high-fidelity inversion capacity. The proposed framework is simple to apply, and we believe it can be easily generalized to other GAN models for future works.

References

- Abdal, R.; Qin, Y.; and Wonka, P. 2019. Image2stylegan: How to embed images into the stylegan latent space? In *Proceedings of the IEEE/CVF International Conference on Computer Vision (ICCV)*.
- Abdal, R.; Qin, Y.; and Wonka, P. 2020. Image2stylegan++: How to edit the embedded images? In *Proceedings of the IEEE/CVF Conference on Computer Vision and Pattern Recognition (CVPR)*.
- Abdal, R.; Zhu, P.; Mitra, N.; and Wonka, P. 2021. StyleFlow: Attribute-conditioned Exploration of StyleGAN-Generated Images using Conditional Continuous Normalizing Flows. In *SIGGRAPH*.
- Alaluf, Y.; Patashnik, O.; and Cohen-Or, D. 2021. ReStyle: A Residual-Based StyleGAN Encoder via Iterative Refinement. *Proceedings of the IEEE/CVF International Conference on Computer Vision (ICCV)*.
- Blau, Y.; and Michaeli, T. 2019. Rethinking lossy compression: The rate-distortion-perception tradeoff. In *International Conference on Machine Learning (ICML)*.
- Bulat, A.; and Tzimiropoulos, G. 2017. How far are we from solving the 2D & 3D Face Alignment problem? (and a dataset of 230,000 3D facial landmarks). In *Proceedings of the IEEE/CVF International Conference on Computer Vision (ICCV)*.
- Chen, C.; Li, X.; Lingbo, Y.; Lin, X.; Zhang, L.; and Wong, K.-Y. K. 2021. Progressive Semantic-Aware Style Transformation for Blind Face Restoration. In *Proceedings of the IEEE/CVF Conference on Computer Vision and Pattern Recognition (CVPR)*.
- Cover, T. M. 1999. *Elements of information theory*. John Wiley & Sons.
- Deng, J.; Guo, J.; Xue, N.; and Zafeiriou, S. 2019. Arcface: Additive angular margin loss for deep face recognition. In *Proceedings of the IEEE/CVF Conference on Computer Vision and Pattern Recognition (CVPR)*.
- Goodfellow, I.; Pouget-Abadie, J.; Mirza, M.; Xu, B.; Warde-Farley, D.; Ozair, S.; Courville, A.; and Bengio, Y. 2014. Generative Adversarial Nets. In *Conference on Neural Information Processing Systems (NeurIPS)*.
- Gu, J.; Shen, Y.; and Zhou, B. 2020. Image processing using multi-code gan prior. In *Proceedings of the IEEE/CVF Conference on Computer Vision and Pattern Recognition (CVPR)*.
- Guan, S.; Tai, Y.; Ni, B.; Zhu, F.; Huang, F.; and Yang, X. 2020. Collaborative learning for faster stylegan embedding. *arXiv preprint arXiv:2007.01758*.
- Guo, J.; Zhu, X.; Yang, Y.; Yang, F.; Lei, Z.; and Li, S. Z. 2020. Towards Fast, Accurate and Stable 3D Dense Face Alignment. In *European Conference on Computer Vision (ECCV)*.
- Harkonen, E.; Hertzmann, A.; Lehtinen, J.; and Paris, S. 2020. GANSpace: Discovering Interpretable GAN Controls. In *Conference on Neural Information Processing Systems (NeurIPS)*.
- Huh, M.; Zhang, R.; Zhu, J.-Y.; Paris, S.; and Hertzmann, A. 2020. Transforming and projecting images into class-conditional generative networks. In *European Conference on Computer Vision (ECCV)*.
- Jahani, A.; Chai, L.; and Isola, P. 2020. On the "steerability" of generative adversarial networks. *The International Conference on Learning Representations (ICLR)*.
- Kang, K.; Kim, S.; and Cho, S. 2021. GAN Inversion for Out-of-Range Images with Geometric Transformations. *Proceedings of the IEEE/CVF International Conference on Computer Vision (ICCV)*.
- Karras, T.; Aila, T.; Laine, S.; and Lehtinen, J. 2018. Progressive growing of gans for improved quality, stability, and variation. *The International Conference on Learning Representations (ICLR)*.
- Karras, T.; Laine, S.; and Aila, T. 2019. A style-based generator architecture for generative adversarial networks. In *Proceedings of the IEEE/CVF Conference on Computer Vision and Pattern Recognition (CVPR)*.
- Karras, T.; Laine, S.; Aittala, M.; Hellsten, J.; Lehtinen, J.; and Aila, T. 2020. Analyzing and improving the image quality of stylegan. In *Proceedings of the IEEE/CVF Conference on Computer Vision and Pattern Recognition (CVPR)*.
- Kingma, D. P.; and Ba, J. 2015. Adam: A method for stochastic optimization. In *The International Conference on Learning Representations (ICLR)*.
- Krause, J.; Stark, M.; Deng, J.; and Fei-Fei, L. 2013. 3D Object Representations for Fine-Grained Categorization. In *International IEEE Workshop on 3D Representation and Recognition*.
- Lu, Y.-D.; Lee, H.-Y.; Tseng, H.-Y.; and Yang, M.-H. 2020. Unsupervised Discovery of Disentangled Manifolds in GANs. *arXiv preprint arXiv:2011.11842*.
- Plummer, A.; Borgne, H. L.; and Hudelot, C. 2020. Controlling generative models with continuous factors of variations. *The International Conference on Learning Representations (ICLR)*.
- Radford, A.; Metz, L.; and Chintala, S. 2016. Unsupervised representation learning with deep convolutional generative adversarial networks. *The International Conference on Learning Representations (ICLR)*.
- Richardson, E.; Alaluf, Y.; Patashnik, O.; Nitzan, Y.; Azar, Y.; Shapiro, S.; and Cohen-Or, D. 2021. Encoding in style: a stylegan encoder for image-to-image translation. *Proceedings of the IEEE/CVF Conference on Computer Vision and Pattern Recognition (CVPR)*.
- Rossler, A.; Cozzolino, D.; Verdoliva, L.; Riess, C.; Thies, J.; and Nießner, M. 2019. Faceforensics++: Learning to detect manipulated facial images. In *Proceedings of the IEEE/CVF International Conference on Computer Vision (ICCV)*.
- Shannon, C. E.; et al. 1959. Coding theorems for a discrete source with a fidelity criterion. *IRE Nat. Conv. Rec*, 4(142-163): 1.

- Shen, Y.; Gu, J.; Tang, X.; and Zhou, B. 2020. Interpreting the latent space of gans for semantic face editing. In *Proceedings of the IEEE/CVF Conference on Computer Vision and Pattern Recognition (CVPR)*.
- Shwartz-Ziv, R.; and Tishby, N. 2017. Opening the black box of deep neural networks via information. *arXiv preprint arXiv:1703.00810*.
- Tishby, N.; Pereira, F. C.; and Bialek, W. 1999. The information bottleneck method. *Proceedings of Annual Allerton Conference on Communication, Control and Computing*.
- Tishby, N.; and Zaslavsky, N. 2015. Deep learning and the information bottleneck principle. In *2015 IEEE Information Theory Workshop (ITW)*, 1–5.
- Tov, O.; Alaluf, Y.; Nitzan, Y.; Patashnik, O.; and Cohen-Or, D. 2021. Designing an encoder for stylegan image manipulation. *ACM Transactions on Graphics (TOG)*, 40(4): 1–14.
- Voynov, A.; and Babenko, A. 2020. Unsupervised discovery of interpretable directions in the gan latent space. In *International Conference on Machine Learning (ICML)*.
- Wang, X.; Li, Y.; Zhang, H.; and Shan, Y. 2021. Towards Real-World Blind Face Restoration with Generative Facial Prior. In *Proceedings of the IEEE/CVF Conference on Computer Vision and Pattern Recognition (CVPR)*.
- Wei, T.; Chen, D.; Zhou, W.; Liao, J.; Zhang, W.; Yuan, L.; Hua, G.; and Yu, N. 2021. A Simple Baseline for StyleGAN Inversion. *arXiv preprint arXiv:2104.07661*.
- Wu, Z.; Lischinski, D.; and Shechtman, E. 2021. StyleSpace Analysis: Disentangled Controls for StyleGAN Image Generation. *Proceedings of the IEEE/CVF Conference on Computer Vision and Pattern Recognition (CVPR)*.
- Xia, W.; Zhang, Y.; Yang, Y.; Xue, J.-H.; Zhou, B.; and Yang, M.-H. 2021. GAN inversion: A survey. *arXiv preprint arXiv:2101.05278*.
- Xu, Y.; Shen, Y.; Zhu, J.; Yang, C.; and Zhou, B. 2021. Generative hierarchical features from synthesizing images. In *Proceedings of the IEEE/CVF Conference on Computer Vision and Pattern Recognition (CVPR)*.
- Yuksel, O. K.; Simsar, E.; Er, E. G.; and Yanardag, P. 2021. LatentCLR: A Contrastive Learning Approach for Unsupervised Discovery of Interpretable Directions. *arXiv preprint arXiv:2104.00820*.
- Zhang, M. R.; Lucas, J.; Hinton, G.; and Ba, J. 2019. Lookahead optimizer: k steps forward, 1 step back. *Conference on Neural Information Processing Systems (NeurIPS)*.
- Zhang, R.; Isola, P.; Efros, A. A.; Shechtman, E.; and Wang, O. 2018. The Unreasonable Effectiveness of Deep Features as a Perceptual Metric. In *Proceedings of the IEEE/CVF Conference on Computer Vision and Pattern Recognition (CVPR)*.
- Zhu, J.; Shen, Y.; Zhao, D.; and Zhou, B. 2020a. In-domain gan inversion for real image editing. In *European Conference on Computer Vision (ECCV)*.
- Zhu, J.-Y.; Krähenbühl, P.; Shechtman, E.; and Efros, A. A. 2016. Generative visual manipulation on the natural image manifold. In *European Conference on Computer Vision (ECCV)*.
- Zhu, P.; Abdal, R.; Qin, Y.; Femiani, J.; and Wonka, P. 2020b. Improved StyleGAN Embedding: Where are the Good Latents? *arXiv preprint arXiv:2012.09036*.
- Zhuang, P.; Koyejo, O.; and Schwing, A. G. 2021. Enjoy Your Editing: Controllable GANs for Image Editing via Latent Space Navigation. *The International Conference on Learning Representations (ICLR)*.

Appendix

A Rate Distortion Theory

Rate-Distortion theory models the lower-bound of compression distortion with a given bit-rate. For source data X , $Y = \text{Encoder}(X)$ is the compressed code (latent code), and $\hat{X} = \text{Decoder}(Y)$ is the reconstructed data. The distortion can be measured by distortion function $D = \mathbb{E}_{P(X, \hat{X})}[\Delta(X, \hat{X})]$, where Δ is ℓ_1 loss in our case. Given a maximum expected distortion D^* , the lower-bound for the bit-rate R is given by:

$$R(D^*) = \min_{D \leq D^*} \{I(X; \hat{X})\}, \quad (8)$$

where $I(X; \hat{X}) = H(X) - H(X | \hat{X})$ is the mutual information between source and reconstruction data. Shannon lower bound is defined as:

$$\begin{aligned} R(D^*) &= \min_{D \leq D^*} \{H(X) - H(X | \hat{X})\} \\ &= H(X) - \max_{D \leq D^*} \{H(X - \hat{X} | \hat{X})\} \\ &\geq H(X) - \max_{D \leq D^*} H(X - \hat{X}). \end{aligned} \quad (9)$$

This shows a larger bit-rate is needed for smaller distortion.

B More Results

B.1 More Qualitative Comparison

We show more inversion and editing results on facial domain in Fig. 9, Fig. 10, Fig. 11, Fig. 12, Fig. 14, Fig. 13, Fig. 15, Fig. 16, Fig. 17, which involve editing on age, smile, eyes, lip, beard and pose. We also show inversion and editing results on car domain in Fig. 18, Fig. 19, Fig. 20 and Fig. 21, which involve editing on color and background. The proposed approach significantly outperforms baselines in terms of both inversion and editing performance.

B.2 Fine-grained Editing

We linearly increase the editing degree α for fine-grained attribute editing. As shown in Fig. 22, the editing results transit smoothly as α changes.

B.3 Video Editing

More qualitative results on video inversion and editing are shown in Fig. 23. Following the pre-processing pipelines of CelebA-HQ and FFHQ, we first detect and crop the face regions from a video, and then use well-trained face image restoration models to improve the video quality (e.g., denoise, super-resolution) as our input.

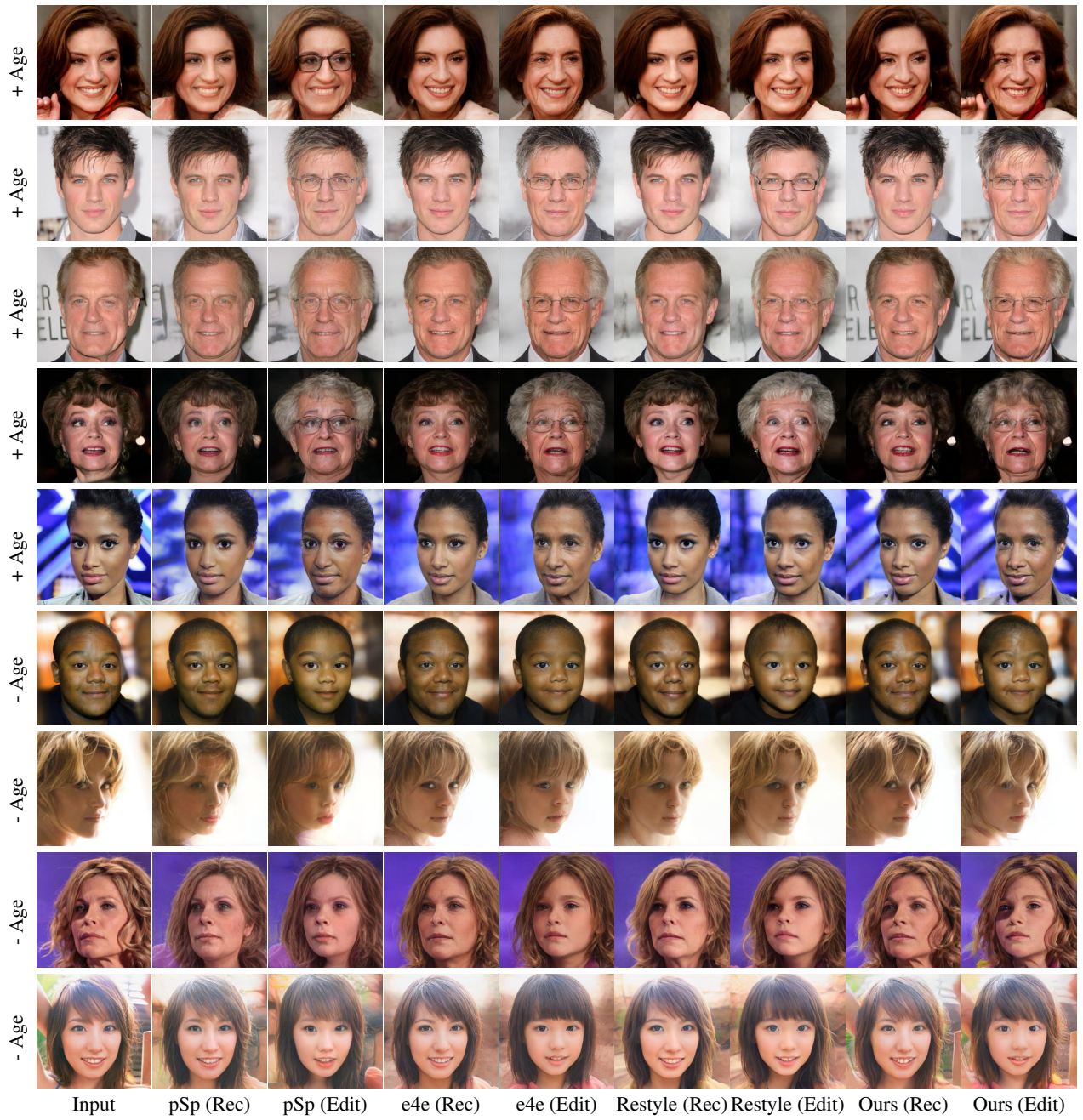


Figure 9: Visual comparisons on Face editing. (Age)

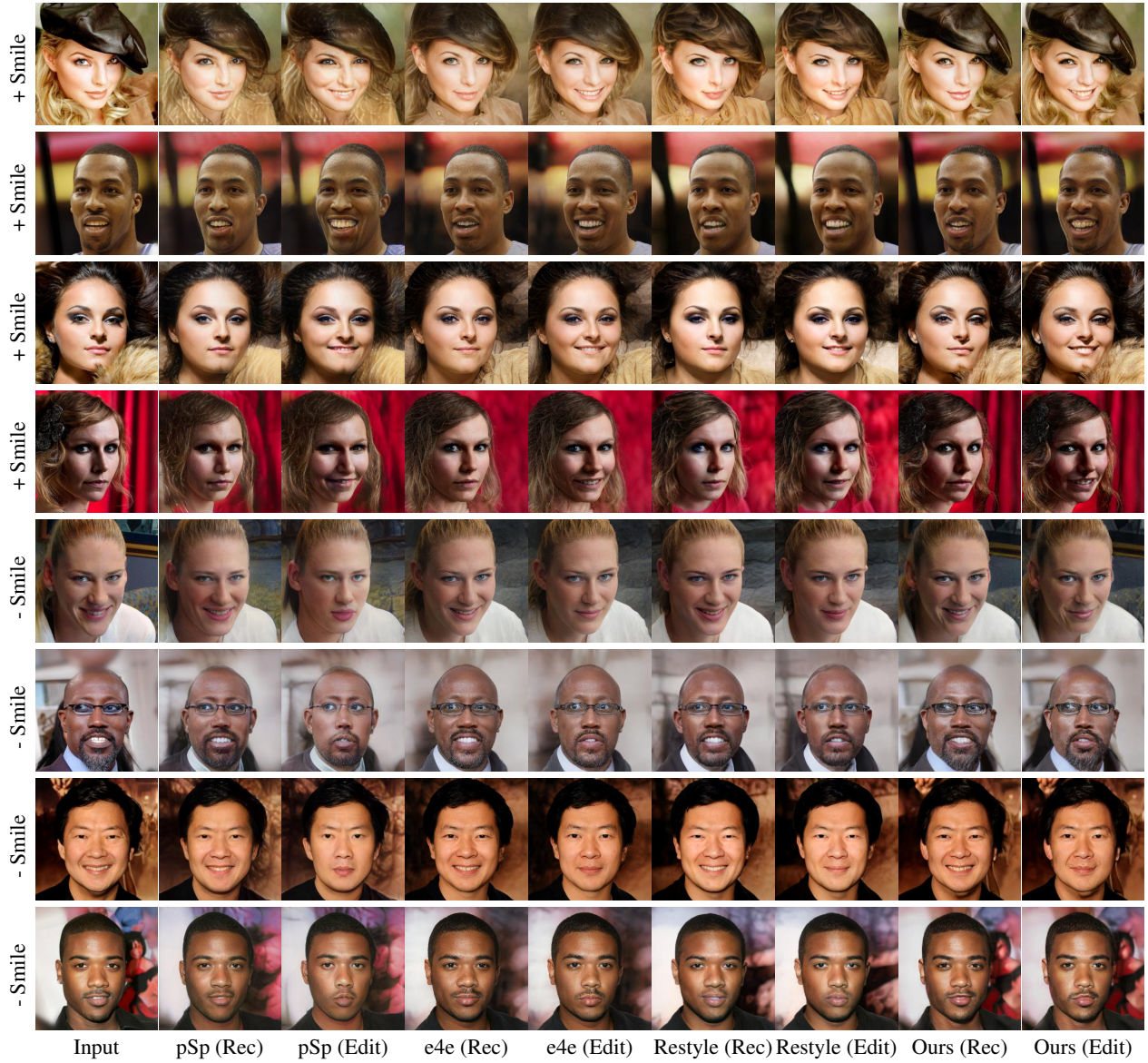
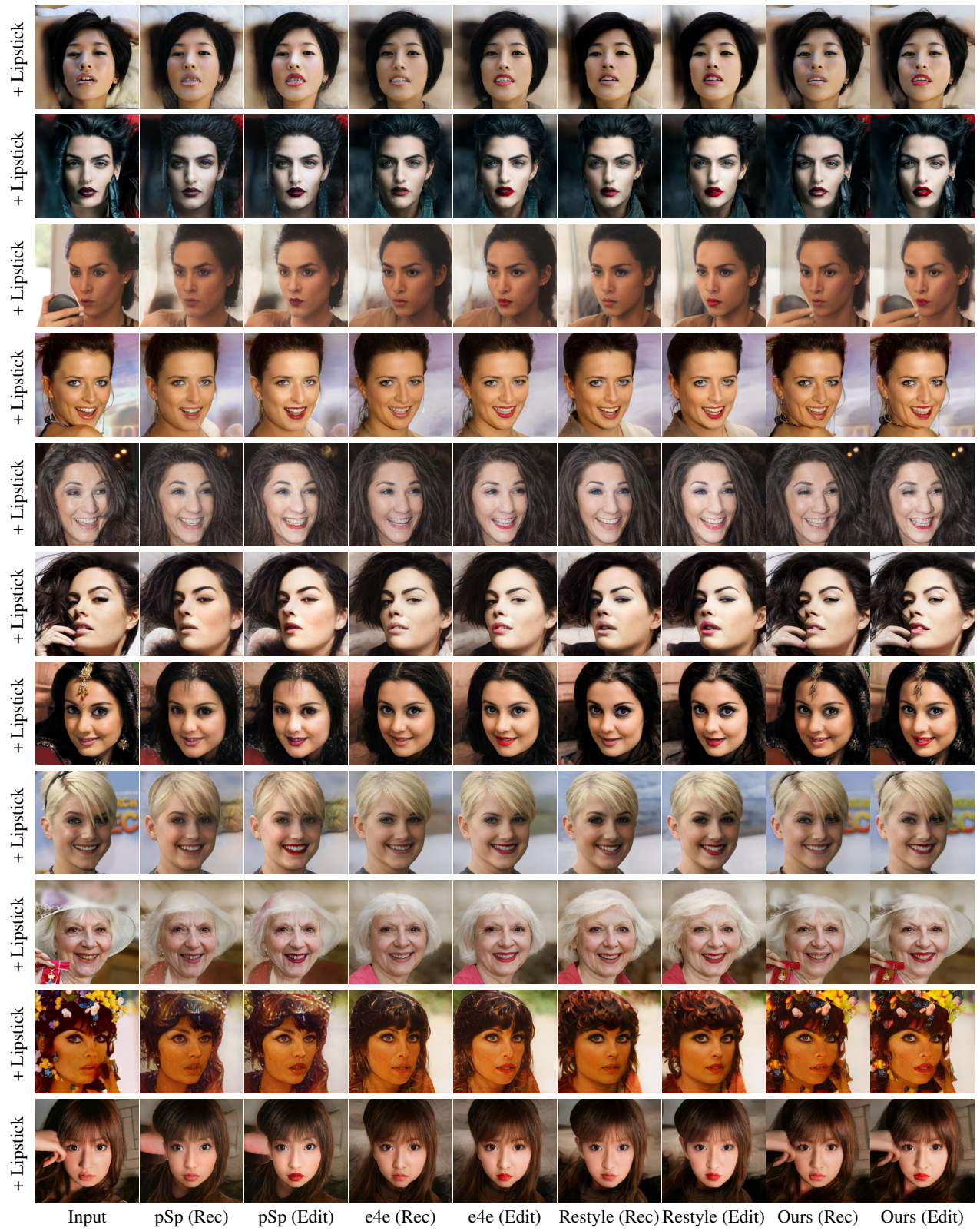


Figure 12: Visual comparisons on Face editing. (Smile)



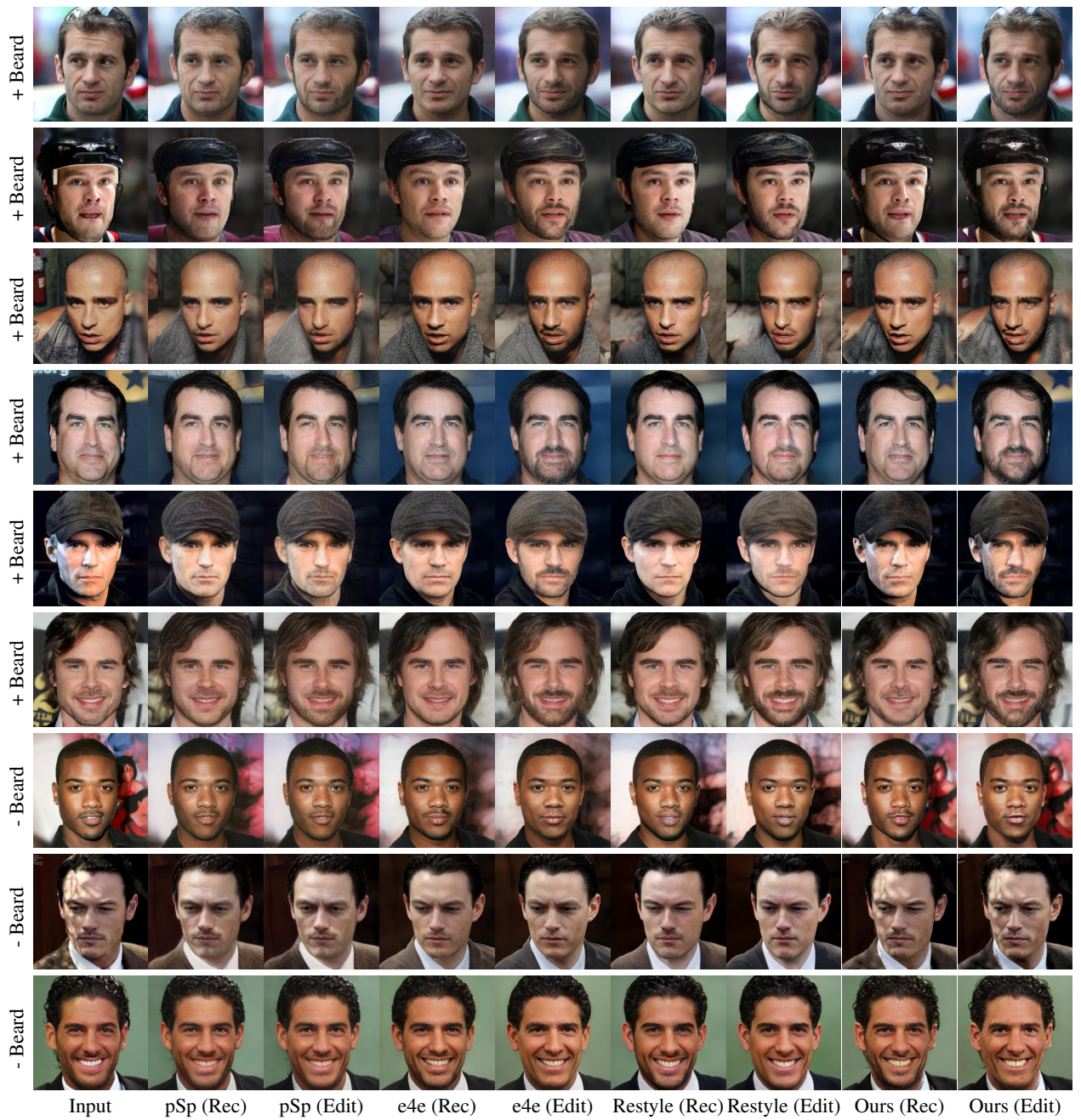


Figure 14: Visual comparisons on Face editing. (Beard)



Figure 15: Visual comparisons on Face editing. (Pose)

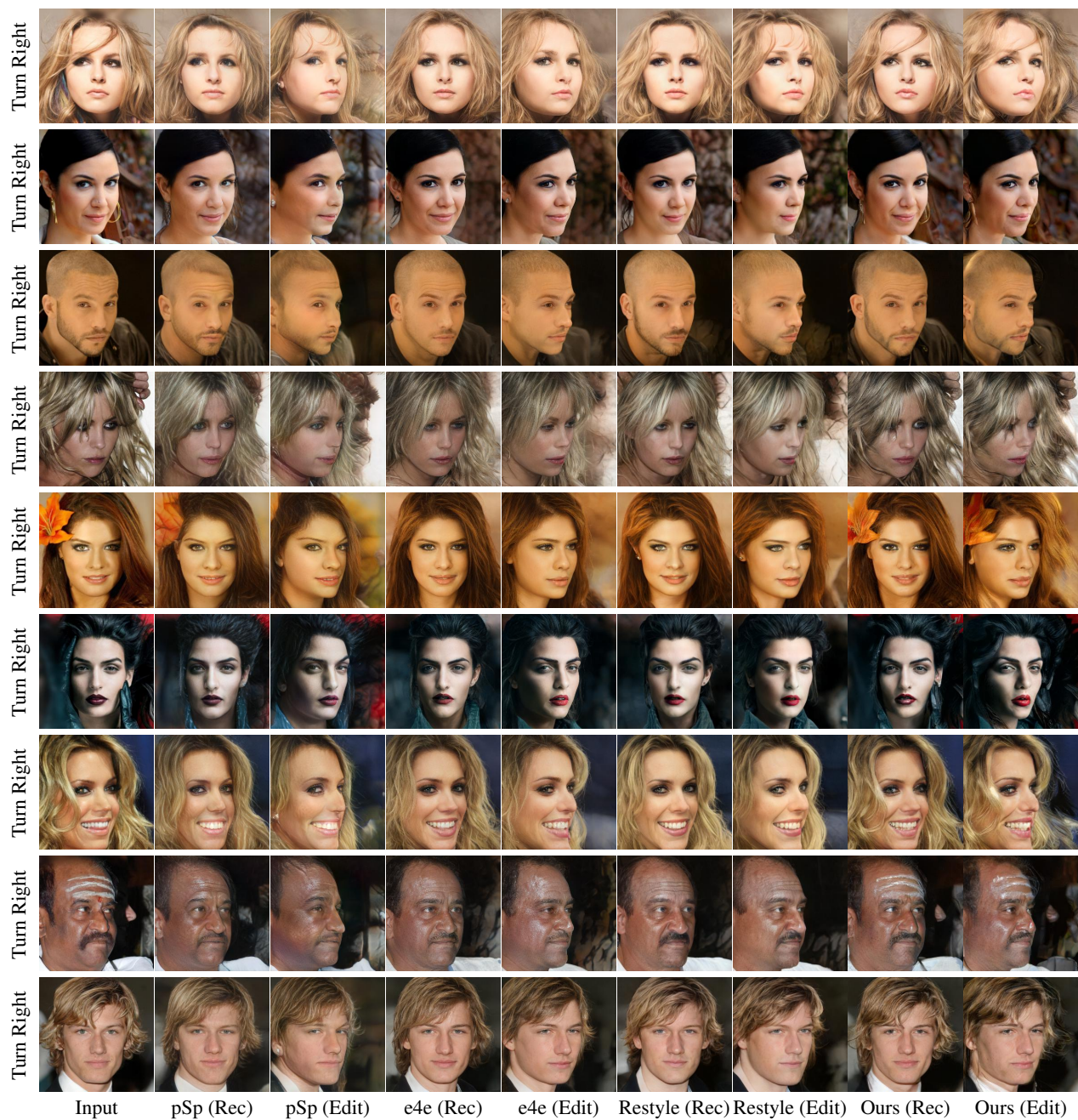


Figure 16: Visual comparisons on Face editing. (Pose)

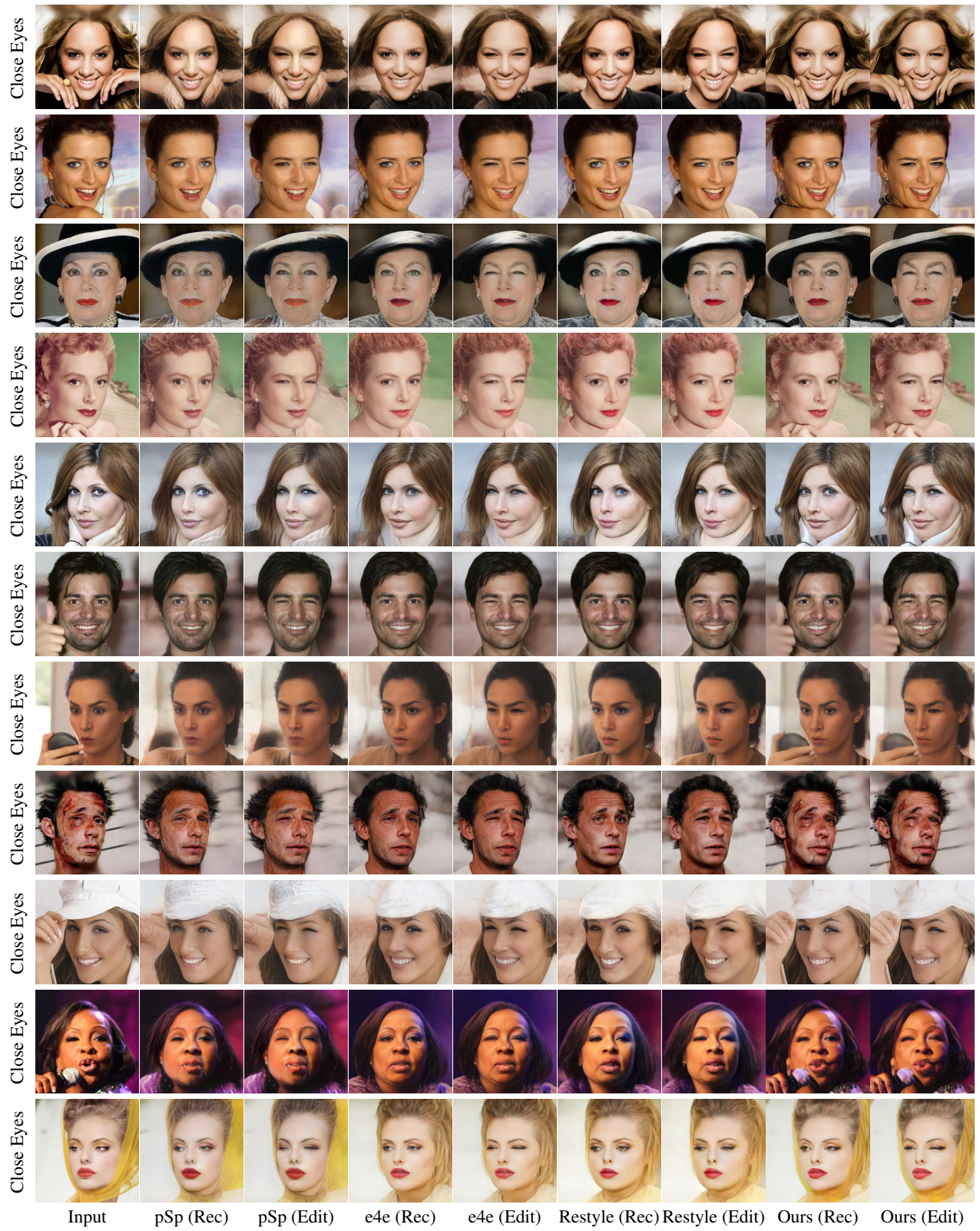


Figure 17: Visual comparisons on Face editing. (Eyes)



Figure 18: Visual comparisons on Car editing. (Color)

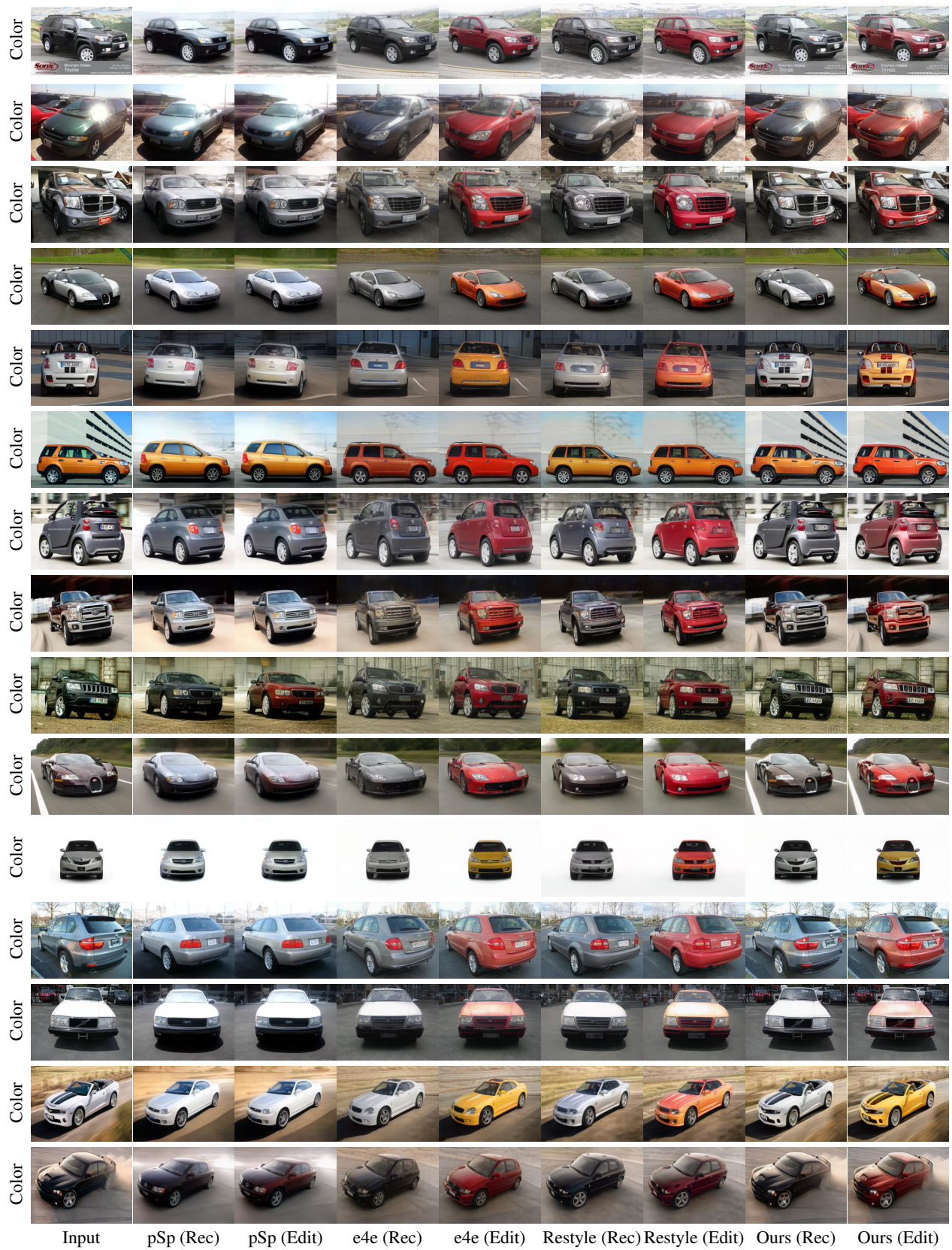


Figure 19: Visual comparisons on Car editing. (Color)

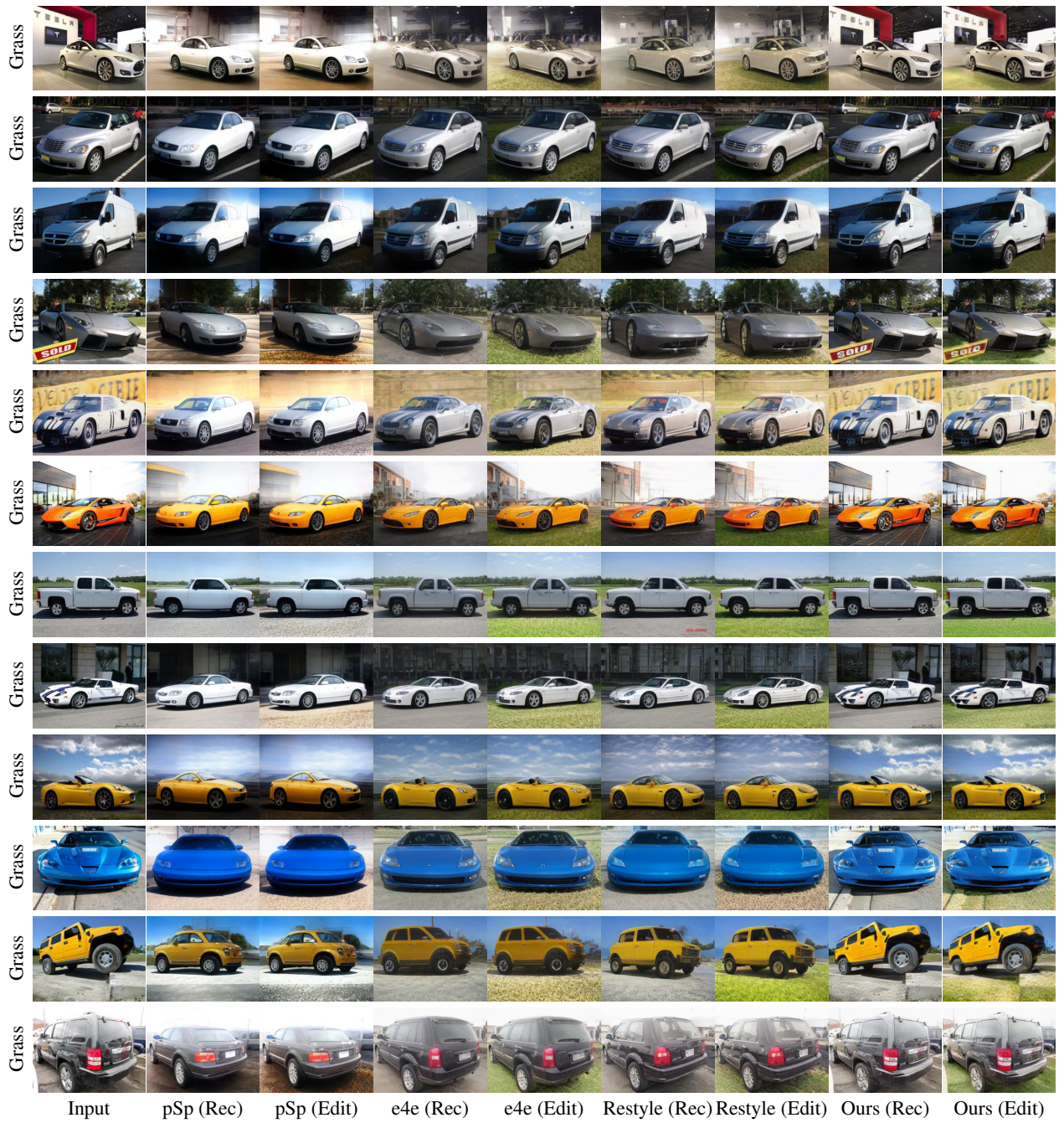


Figure 20: Visual comparisons on Car editing. (Grass)

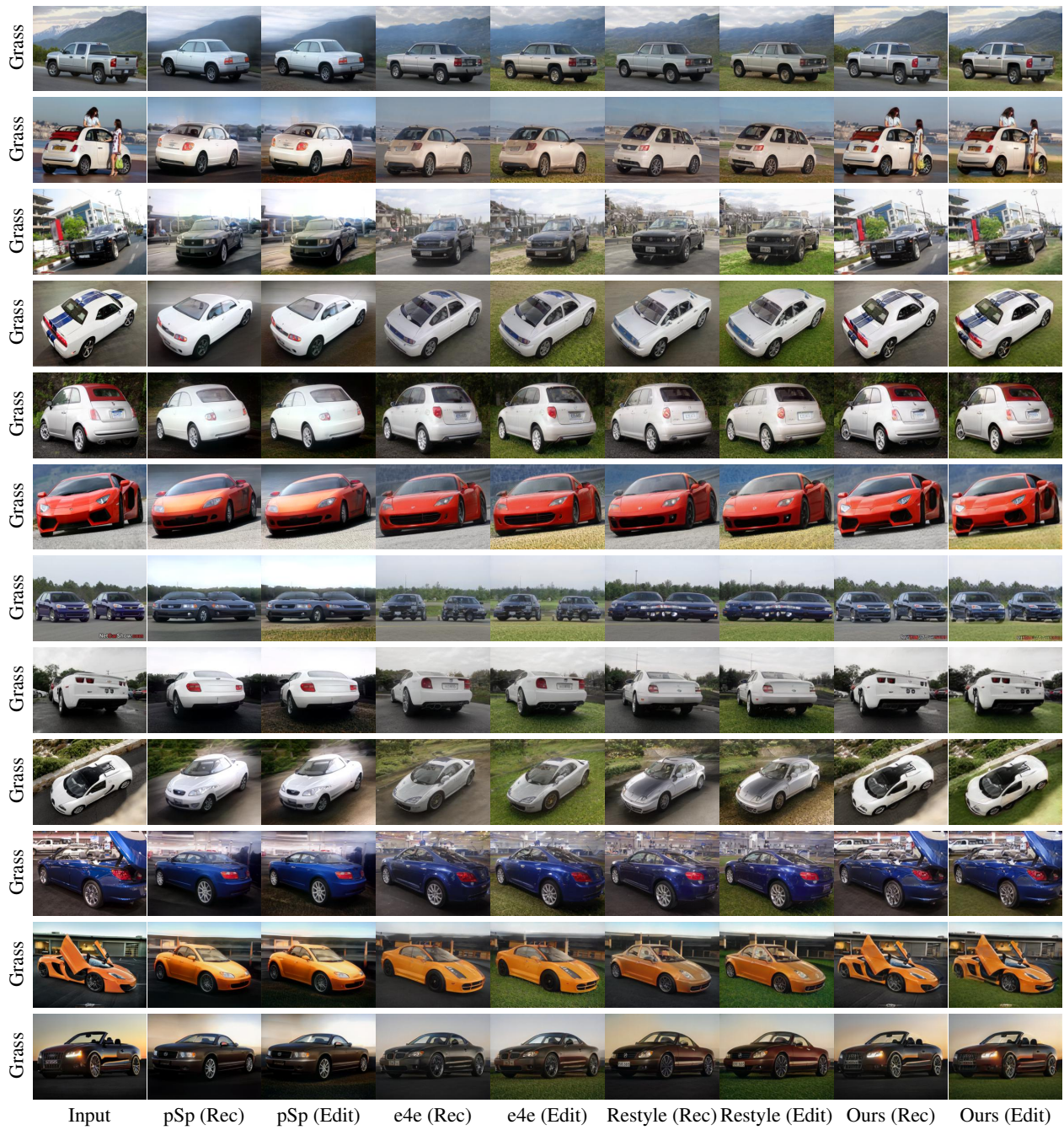


Figure 21: Visual comparisons on Car editing. (Grass)



Figure 22: Results of fine-grained attribute editing. We linearly interpolate the editing degree α and perform editing.



Figure 23: Results of inversion and editing (+ age and + smile) on videos.